Effects of Al Content and Synthesis Temperature on Al-Substituted Fe Oxides: Crystal Properties and Fe(III) Bioaccessibility

Tongxu Liu,[1] Xiaomin Li,[1] Fangbai Li,[1] Liang Tao,[1] and Hong Liu[2]

Abstract: Four series of Al-substituted Fe oxides with different Al contents were synthesized under different temperatures and characterized to study the effects of Al substitution on the crystal properties and bioaccessibility of Fe oxides. The UV-visible diffuse-reflectance spectra and their first derivatives showed that color changes from red to white were associated with the visible absorbance of Fe oxides and Al oxides. The X-ray diffraction results showed that the presence of Al in Fe oxides could hinder the formation of maghemite and hematite in addition to the crystal transformation from maghemite to hematite during sintering. The Brunauer-Emmett-Teller surface areas of Al-substituted Fe oxides increased with increasing Al content and with decreasing sintering temperatures. Fourier transform infrared spectra results showed that gibbsite formed with high Al contents. The crystal structure, crystallinity, and the surface area of Al-substituted Fe oxides heavily depended on the Al content and the sintering temperature. The effects of Al on the hydroxylamine-reducible Fe(III) of Al-substituted Fe oxides were also investigated. The results showed that the hydroxylamine-reducible Fe(III) of Al-substituted Fe oxides increased with increasing Al content for the Fe oxides with a high degree of crystallization when synthesized at higher temperatures (>300°C) but decreased with increasing Al content for Fe oxides with a low sintering temperature (180°C). The effect of the Al content on hydroxylamine-reducible Fe(III) was attributable to the crystal structure, crystallinity, and the properties of surface structures—all of which can provide detailed information needed to understand the effect of Al on the iron reactivity of natural soils or sediments.

Key Words: Al content, temperature, iron oxides, crystal properties, Fe(III) bioaccessibility

(*Soil Sci* 2014;179: 468–475)

Iron is the fourth most abundant element in the earth's crust, and it is essential to nearly all known organisms (Lovley et al., 2004). Red soil, a type of iron-rich soil, is very important in China. It covers 21% of the total land area, holds 40% of the population capacity, and contributes 50% of the gross domestic product of China. The redox transformation of iron plays a key role in the fate of heavy metals (Lovley et al., 2004; Li et al., 2012b), humic substances (Li et al., 2013, 2014; Wu et al., 2014), and organic contaminants (Li et al., 2010; Cao et al., 2012) in soil and sediments. Particularly, the iron redox cycling affects several natural processes in red soil, such as soil acidification (Li and Xu, 2013), nutrient transport (Gerke, 2010; Zhang et al., 2012, 2014), and mineralization (Kappler and Straub, 2005; Liu et al., 2011).

Iron (hydr)oxides are known to exist rarely as pure phases in natural environments, but they often contain a variety of metal impurities (Cornell and Schwertmann, 2003). Aluminum, which is one of the most abundant elements in soils and sediments, is commonly coprecipitated with iron in natural Fe(III) (hydr)oxides. Iron and Al oxides and oxyhydroxides are common minerals in soil and surface and groundwater environments (Bazilevskaya et al., 2011). The omnipresence of aluminum as a product of weathering results in most natural Fe(III) (hydr)oxides being Al substituted (Cornell and Schwertmann, 2003). Aluminum substitutions of up to 33% (mole Al/mole Al + Fe) have been found in natural goethite minerals, with up to 16% in hematite and up to 9.5% in lepidocrocite (Wang et al., 1999). Aluminum coprecipitation in ferrihydrite has been observed in nature and has been synthesized in the laboratory (Cornell and Schwertmann, 2003) to contain up to 20 mol% Al without forming separate Al phases (Masue et al., 2007). Aluminum substitution can impact the properties of Fe(III) (hydr)oxides, including the unit-cell edge length and volume of the Fe(III) (hydr)oxide (Cornell and Schwertmann, 2003), average crystallite size, particle morphology, surface area, solubility (Trolard and Tardy, 1987; Bonneville et al., 2004), surface chemistry (Feng and Yapp, 2009), and rates of acid and reductive dissolution (Cornell and Schwertmann, 2003).

Given that Al substitution in Fe(III) (hydr)oxides can significantly change the physical and chemical properties of Fe(III) (hydr)oxides, it is important to understand how Al substitution will affect bacterial Fe(III) reduction and dissolution. To date, there have only been a few published studies to explore the effects of Al substitution within ferrihydrite or lepidocrocite on bacterial reduction (Ekstrom et al., 2010). The results from four published studies on the bacterial reduction and dissolution of Al-goethites found contrasting results, with Al substitution resulting in decreased Fe(III) reduction (Bousserrhine et al., 1999; Dominik et al., 2002), increased microbial productivity (Maurice et al., 2000), or no substantial change in the extent and rate of reduction (Kukkadapu et al., 2001). These findings highlight the need for a broader investigation on the impact of Al substitution within Fe (III) (hydr)oxides on microbial Fe(III) reduction. However, previous studies focused on Al-substituted Fe oxides with Al contents less than 33% and lower crystallinity (ferrihydrite, lepidocrocite, and goethite) (Wang et al., 1999; Hansel et al., 2011; Cristina et al., 2012; Bazilevskaya et al., 2012), but the effects of a high proportion of Al remain unclear.

The crystallinity of Fe oxides in soils is one of the most important physicochemical parameters in evaluating the iron bioaccessibility of iron-bearing minerals. Because of the influence of a series of natural and artificial processes, the crystallinity of Fe oxides in soils usually varies dramatically in different environments

[1]Guangdong Key Laboratory of Agricultural Environment Pollution Integrated Control, Guangdong Institute of Eco-Environmental and Soil Sciences, Guangzhou, China.
[2]Chongqing Institute of Green and Intelligent Technology, Chinese Academy of Sciences, Chongqing, China.
Address for correspondence: Dr. Tongxu Liu, Guangdong Key Laboratory of Agricultural Environment Pollution Integrated Control, Guangdong Institute of Eco-Environmental and Soil Sciences, Guangzhou, 510650, China. E-mail: txliu@soil.gd.cn or liuhong@cigit.ac.cn
Financial Disclosures/Conflicts of Interest: *This work was funded by the National Natural Science Foundations of China (nos. 41471216, 41340018, and 41271248) and the Natural Science Foundation of Guangdong Province, China (S2011030002882).*
Received February 18, 2014.
Accepted for publication December 12, 2014.

ISSN: 0038-075X
DOI: 10.1097/SS.0000000000000092

(Lair et al., 2009; Li and Richter, 2012). Other Fe oxides or oxyhydroxides, such as maghemite (γ-Fe_2O_3), hematite (α-Fe_2O_3), and magnetite (Fe_3O_4), naturally exist in the earth's crust as well (Cornell and Schwertmann, 2003). Unfortunately, such crystal properties are very difficult to observe directly and to measure in the pedoenvironment because soil iron minerals consist of very small Fe oxide crystallites and are often present at low concentrations (Crosa et al., 1999). The influence of Al substitution on the reactivity of these Fe oxides with different crystal structures and crystallinity still remains unclear in natural soils and sediments either.

To clearly illustrate the effects of high Al content and crystallinity on the crystal properties and Fe(III) bioaccessibility of Fe oxides, Al-Fe oxides with different Al content and crystallinity were synthesized under different temperatures (Liu et al., 2013) and used as the model Fe oxides in natural soil environments. The synthesized Al-Fe oxides were systematically characterized by X-ray diffraction (XRD), diffuse-reflectance spectra (DRS), Fourier transform infrared (FTIR), and Brunauer-Emmett-Teller (BET). Hydroxylamine-reducible iron was also examined as an indicator of iron bioaccessibility. The results could provide fundamental information for understanding natural Al and Fe interactions in the geochemistry of soil minerals and the bioaccessibility of natural soil minerals.

MATERIALS AND METHODS

Materials

$Fe(NO_3)_3 \cdot 9H_2O$ (≥99.0%), $Al(NO_3)_3 \cdot 9H_2O$ (≥98.0%), and glycol (99.7%) were purchased from the Guangzhou Chemical Reagent Factory in China. Hydroxylamine hydrochloride ($NH_2OH \cdot HCl$, 99%) and 1,10-phenanthroline (99%) were purchased from Sigma-Aldrich and used without further purification.

Synthesizing Al-Substituted Fe Oxide Powders

Pure Fe oxide powders were prepared from $Fe(NO_3)_3 \cdot 9H_2O$ and glycol by a sol–gel procedure in which 0.1 mol $Fe(NO_3)_3 \cdot 9H_2O$ was added into 160 mL of glycol and stirred until dissolved; the solution was then refluxed in a 250-mL flask at 65°C for 24 h to obtain hydrosol. The hydrosol was dried at 100°C for 24 h to obtain a xerogel, and the xerogel was then ground and sintered at 180°C, 300°C, 420°C, and 550°C for 2 h. Four series of Al-substituted Fe oxide powders were then prepared from $Fe(NO_3)_3 \cdot 9H_2O$, $Al(NO_3)_3 \cdot 9H_2O$, and glycol by following a similar procedure in which a 0.1-mol $Fe(NO_3)_3 \cdot 9H_2O$ and $Al(NO_3)_3 \cdot 9H_2O$ mixture was dissolved into 160 mL of glycol with different molar ratios of Al/(Fe + Al) (x, %). The Al-substituted Fe oxide powders with different alumina contents (x = 10%~90%) were sintered at 180°C, 300°C, 420°C, and 550°C for 2 h.

Characterizing Al-Substituted Fe Oxide Powders

The spectral properties of all the powders were characterized by a UV-visible diffuse reflectance spectrometer (Varian 100) within the range of 200 to 800 nm. To determine the crystal-phase composition of the prepared Al-Fe oxides, an XRD measurement was performed at room temperature using a Rigaku D/MAX-IIIA diffractometer with Cu Kα radiation (λ = 0.15418 nm). The phases were identified by comparing their diffraction patterns with those of the standard powder XRD cards compiled by the Joint Committee on Powder Diffraction Standards (Schwertmann and Cornell, 1991). An accelerating voltage of 35 kV and an emission current of 30 mA were used. The BET surface areas of all samples were measured by the BET method, in which an N_2 adsorption at 77 K was applied using a Carlo Erba Sorptometer. Fourier transform infrared spectra of the Al-Fe oxides were also recorded with an FTIR spectrometer (Perkin Elmer) at room temperature.

Experimental Procedure for Fe(III) Reduction by Hydroxylamine Hydrochloride

In the present study, the concentration of hydroxylamine-reducible Fe(III) is considered to be an indicator of available Fe (III) for different Al-Fe oxides because it has a strong relation with the extent of microbial Fe(III) reduction in aquifer sediments (Lovley and Phillips, 1987). The hydroxylamine-reducible Fe(III) in Fe oxides was measured using hydroxylamine hydrochloride (0.25 mol L^{-1} $NH_2OH \cdot HCl$) (Li et al., 2012a; Zhang et al., 2014), and the solid content of total Fe was fixed at 25 mmol L^{-1} for all Al-Fe oxides. The experimental procedure was as follows: Al-Fe oxide powder with 0.5 mmol Fe (0.04 g Fe_2O_3) was preweighed into each test serum bottle (25 mL). The $NH_2OH \cdot HCl$ solution was purged with O_2-free argon gas for 2 h before the $NH_2OH \cdot HCl$ solution and serum bottles with powders were transferred to an anaerobic chamber, in which standard anaerobic techniques were used in the following experimental procedure. Then the serum bottles were filled with 20 mL of 0.25 mol L^{-1} $NH_2OH \cdot HCl$ solution. Last, the serum bottles were sealed with Teflon-coated butyl rubber stoppers and crimp seals. All studies were conducted in duplicate, with vials incubated in a shaker at 180 r.p.m. and 25°C. To determine the hydroxylamine-reducible Fe(III), samples (0.5 mL) were taken and filtered through a 0.22-μm syringe filter before analysis. Dissolved Fe(II) was measured by the 1,10-phenanthroline colorimetric method. All manipulations related to preparing the samples for Fe(II) determination by 1,10-phenanthroline were conducted inside the anaerobic chamber before colorimetric measurements.

RESULTS AND DISCUSSION

Effect of Al on the Spectral Properties of Al-Fe Oxides

The surfaces of Al-Fe oxides gradually changed with the changing Al content and temperature. This effect was first indicated by a visible color change in the synthetic powders. The color changed from red to white with increasing Al content for all treatments under different fixed temperatures. For the sample with a fixed Al content, the color became darker as the synthesis temperatures increased. Torrent and Barron (2003) reported a relation between the DRS spectrum and the color of natural and synthetic hematites. To compare the differences of all Al-Fe oxide samples, the DRS spectra of all the powder samples were measured. The results in Figure 1 show that all the samples exhibited a strong absorption in the visible region (400–750 nm), and the optical absorption decreased gradually as the Al content increased in the Al-Fe oxides, indicating that the strong optical absorption was primarily attributed to the Fe in the Al-Fe oxides; adding Al diluted the proportion of Fe on the surface of the bulk composite oxides.

Several peaks in the range of 400 to 750 nm were observed for all the Fe oxide samples. It was difficult to distinguish among them. The detection and elimination of different sources of error from the analyte reference solution is a continuous process in analytical chemistry, especially for spectral analysis (Verdú-Andrés et al., 1998). The first or second derivative data between the sample and an analyte reference solution at each wavelength are normally used to magnify the signal of the target peaks and eliminate the background (Wahbi et al., 2007). To provide a clear illustration of individual peaks among all the samples, the first-order derivatives of the absorbance versus the wavelength were calculated by using a cubic spline procedure in OriginPro version

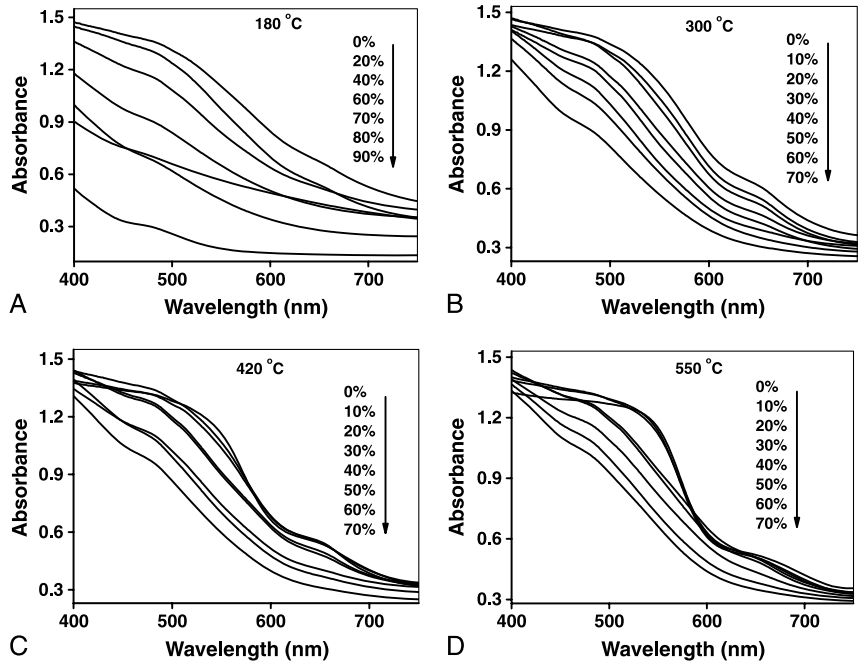

FIG. 1. UV-visible diffuse-reflectance spectra of Al-Fe oxides with different Al/(Al + Fe) molar percentages synthesized at different temperatures: (A) 180°C, (B) 300°C, (C) 420°C, and (D) 550°C.

8.0. The results in Figure 2 show two peaks at approximately 465 nm and 636 nm, which indicated similar changing trends for all the samples. The peak at approximately 465 nm increased gradually with increasing Al content, indicating that the peak could be attributed to Al oxides. The peak at approximately 636 nm decreased gradually with increasing Al content, indicating that the peak could be attributed to Fe oxides.

Effect of Al on the Crystal Properties of Al-Fe Oxides

To investigate the effects of temperatures and Al contents on the crystal properties, the XRD patterns of all the samples were measured. The patterns for all the Al-Fe oxides are shown in Figure 3. For the samples synthesized at 180°C (Fig. 3A),

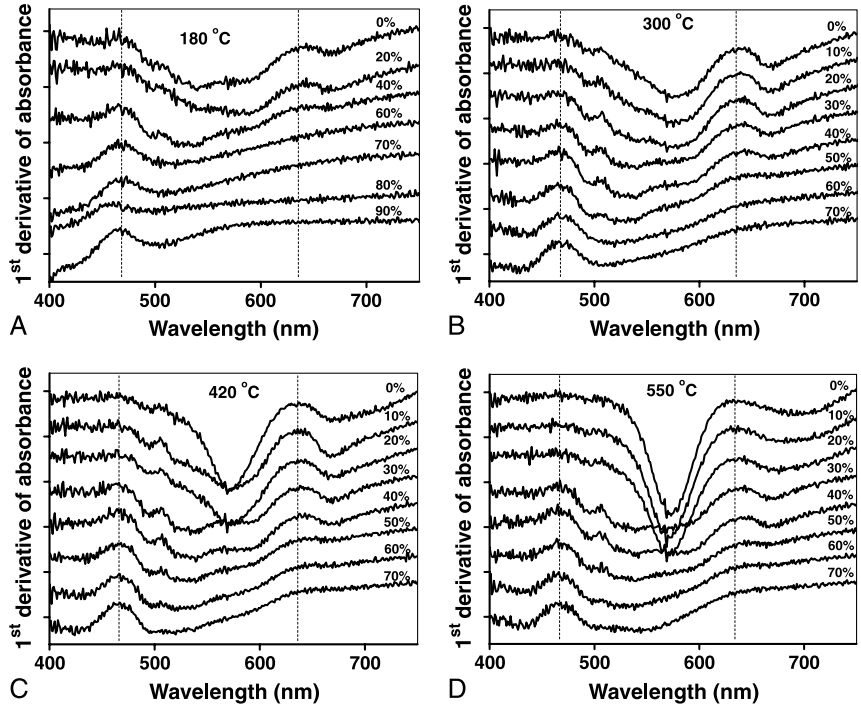

FIG. 2. The first derivatives for the absorbance of UV-visible diffuse-reflectance spectra in Figure 1 for Al-Fe oxides with different Al/(Al + Fe) molar percentages synthesized at different temperatures: (A) 180°C, (B) 300°C, (C) 420°C, and (D) 550°C.

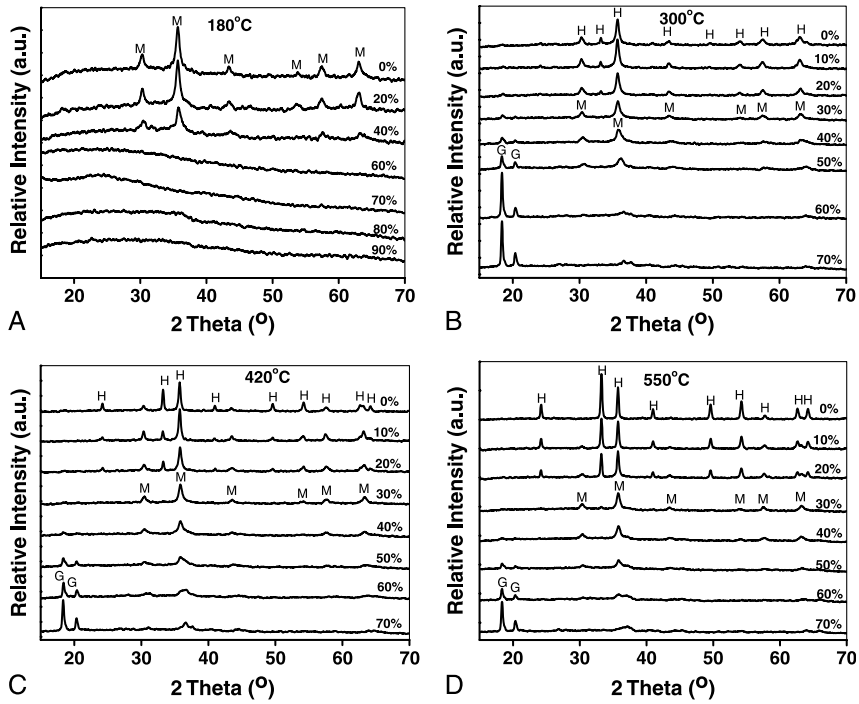

FIG. 3. X-ray diffraction patterns of Al-Fe oxides with different Al/(Al + Fe) molar percentages synthesized at different temperatures: (A) 180°C, (B) 300°C, (C) 420°C, and (D) 550°C. M indicates maghemite; H, hematite; G, gibbsite.

Al-Fe oxide samples exhibited dominant peaks at 30.3, 35.7, 57.3, and 63.0 degrees, which are primarily attributed to maghemite based on the Joint Committee on Powder Diffraction Standards (Bazilevskaya et al., 2011). The Al-Fe oxide samples (Fig. 3B) exhibited a new peak at 33.2 degrees because of the presence of hematite. This peak increased significantly for the samples that were sintered at 420°C (Fig. 3C) and 550°C (Fig. 3D), indicating a mixed crystal structure of maghemite and hematite. The peak at 24.2 degrees in Figure 3C and D further confirmed the increasing formation of hematite with increasing temperatures. The peaks at 18.4 and 20.3 degrees were attributed to the presence of gibbsite ($Al(OH)_3$) (Bazilevskaya et al., 2011). It is clear that the gibbsite was not formed at a low temperature (180°C). The peak intensities of gibbsite increased with increasing Al content in Al-Fe oxides at 300°C, 420°C, and 550°C.

To demonstrate changes in the crystal structure and crystallinity with Al content and temperature, the peaks at 35.7, 30.3, 33.2, and 18.4 degrees for all the samples were plotted as a function of Al content, which reflect the crystallinity of γ-Fe_2O_3 + α-Fe_2O_3, γ-Fe_2O_3, α-Fe_2O_3, and $Al(OH)_3$, respectively. The results in Figure 4A showed that the peak intensities at 35.7 degrees decreased gradually as the proportion of Al increased in the Al-Fe oxides, indicating that introducing alumina could delay the crystallization of γ-Fe_2O_3 (180°C) and the mixed structure γ-Fe_2O_3 + α-Fe_2O_3 (300°C, 420°C, and 550°C). The results also showed that the peaks increased as the synthesis temperature increased during the sintering treatment, indicating that the high temperature could facilitate the crystallization of composite oxides. The results in Figure 4B showed that peaks at 30.3 degrees were attributable to γ-Fe_2O_3 alone. The suggested crystallinity of γ-Fe_2O_3 increased with increasing Al content at the beginning (0%–20% for 180°C, 0%–10% for 300°C and 420°C, and 0%–30% for 550°C) and then decreased gradually with high Al contents. This result indicates that the incorporation of low Al content can facilitate the crystallization of γ-Fe_2O_3, but high Al content inhibited the crystallization process. The results in Figure 4C showed that the peaks at 33.2 degrees were attributable to α-Fe_2O_3 alone. The peak intensities decreased gradually with the increasing proportion of Al in the Al-Fe oxides, indicating that the introduction of Al significantly delays the crystallization of α-Fe_2O_3. The peak intensity with the same Al content was also shown to increase with increasing synthesis temperature, indicating that the high temperature could cause the increase of the crystallinity of hematite. On the one hand, Al addition inhibited the direct crystallization process of α-Fe_2O_3. On the other hand, the fact that γ-Fe_2O_3 increased with increasing Al content for low Al content (Fig. 4B) could also hinder the crystal transformation of Fe oxides from maghemite to hematite during the sintering treatment, resulting in a further delay of the α-Fe_2O_3 crystallization process. The results in Figure 4D show that the peaks at 18.4 degrees were attributable to $Al(OH)_3$. No significant peaks were observed for samples synthesized below 180°C, suggesting that Al $(OH)_3$ was not formed under those conditions. The peak intensities at 18.4 degrees increased gradually with the increasing Al content of Al-Fe oxides at 300°C, 420°C, and 500°C, revealing that a high temperature is favorable for the $Al(OH)_3$ crystallization process.

The transformation from $Fe(OH)_3$ to Fe_2O_3 predominantly occurs at the temperature of 109°C to 140°C (Melnikov et al., 2014). γ-$Al(OH)_3$ can lose part of its crystalline water at 270°C to 317°C but does not change into Al_2O_3 until the system is above 700°C (Zhu et al., 2010). In this study, the synthesized temperatures of Al-Fe oxides (180°C–550°C) were higher than the dehydration temperature of $Fe(OH)_3$ but lower than that of $Al(OH)_3$. Therefore, the main composition of the Al-Fe oxides includes dehydrated Fe_2O_3 and hydrated $Al(OH)_3$. The crystallinity of Al $(OH)_3$ under 300°C was slightly higher than it was at 420°C and 500°C, indicating that $Al(OH)_3$ was decomposed or dehydrated under higher temperatures (420°C and 500°C).

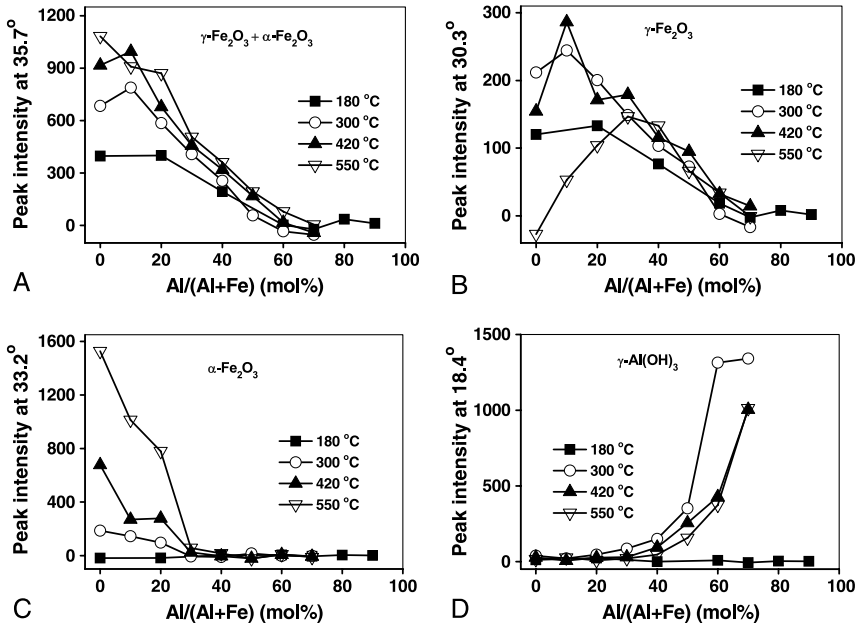

FIG. 4. Peak intensities at (A) 2θ = 35.7 degrees, (B) 2θ = 30.3 degrees, (C) 2θ = 33.2 degrees, and (D) 2θ = 18.4 degrees derived from the X-ray diffraction patterns in Figure 3 as a function of the Al content for all Al-Fe oxide samples.

Effect of Al on the Chemical State of Al-Fe Oxides

To investigate the effect of the Al content and temperature on the chemical state of Al-Fe oxides, FTIR absorbance spectra from 4,000 to 650 cm^{-1} were examined for all the samples. The results in Figure 5A show that the broad peaks in the 3,350 to 3,450 cm^{-1} range were attributable to the O–H stretching vibration of water and an OH group on the surface of Al-Fe oxides. The peak at 692 cm^{-1} could be explained by the Fe–O vibration of hematite or maghemite (Fysh and Fredericks, 1983), which was only observed in the samples with low Al contents (<30%) synthesized at high temperatures (>300°C). The peak at 692 cm^{-1} disappeared for all the samples with a sintering temperature of 180°C and in the samples with Al contents greater than 30%. The results in Figure 5B to D show that the peaks at 730, 971, 1,019, 3,371,

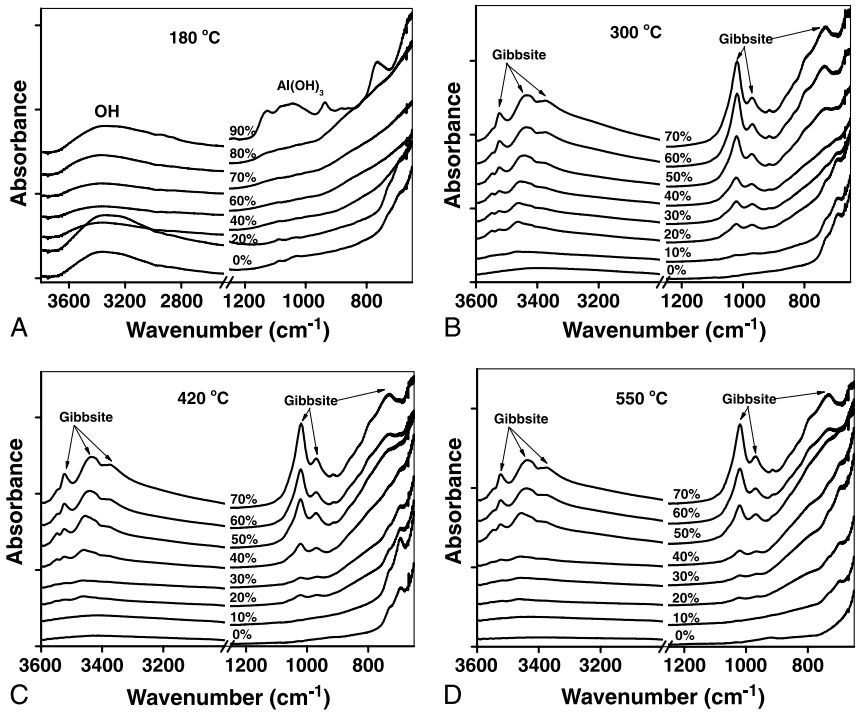

FIG. 5. Fourier transform infrared spectra of Al-Fe oxides with different Al/(Al + Fe) molar percentages synthesized at different temperatures, (A) 180°C, (B) 300°C, (C) 420°C, and (D) 550°C.

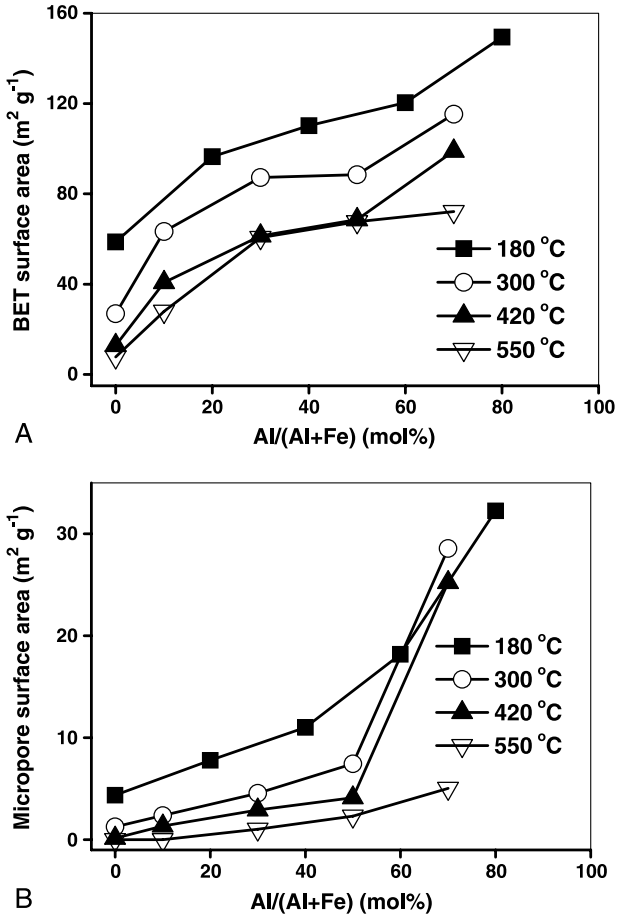

FIG. 6. Brunauer-Emmett-Teller surface areas (A) and micropore surface areas (B) of Al-Fe oxides with different Al/(Al + Fe) molar percentages synthesized at different temperatures: 180°C, 300°C, 420°C, and 550°C.

3,442, and 3,522 cm^{-1} were observed for Al contents higher than 20% (300°C), 40% (420°C), and 50% (550°C), which is attributable to the Al–O vibration of gibbsite ($Al(OH)_3$) (Bazilevskaya et al., 2011), indicating that high temperatures were favorable for the gibbsite crystallization process, but gibbsite may be decomposed or dehydrated under high temperatures (420°C and 500°C). This result is consistent with the XRD patterns.

The Effect of Al on the BET Surface Areas of Al-Fe Oxides

The BET surface areas of different Al-Fe oxides were determined as shown in Figure 6A. It is clear that the BET surface areas of all oxide samples are substantially affected by both the Al content and sintering temperature. The microporosity of Al-Fe oxides was further analyzed from the BET data, with the micropore surface areas of Al-Fe oxides plotting as a function of Al/(Al + Fe) molar percentage (Fig. 6B). The micropore surface areas of Al-Fe oxides increased gradually with increasing Al content. Because Al oxides can be activated under higher temperature, yielding enormous internal surfaces for adsorption, the increasing BET surface areas of Al-Fe oxides may be mainly attributed to the newly formed micropores in the Al-Fe oxides with increasing Al content. For the samples with the same Al content, both BET and micropore surface areas of Al-Fe oxides decreased with increasing sintering temperature, which should be caused by the increase in crystallinity (Fig. 4) and decrease in micropore caused by the higher sintering temperature.

The Effect of Al on the Hydroxylamine-Reducible Fe(III) in Al-Fe Oxides

Fe(III) oxyhydroxide bioaccessibility correlated with its solubility, which seems to be the rate-controlling factor in biotic Fe (III) reduction by *Shewanella putrefaciens* 200R (Bonneville et al., 2004). However, the solubility products of Fe(III) oxyhydroxides reported in the literature often vary by several orders of magnitude. Lovley and Phillips (1987) have suggested that the hydroxylamine extraction procedure is a more selective indicator of microbially reducible Fe(III) bioaccessibility than the oxalate extraction method. They also found a strong relation between the amount of hydroxylamine-extractable Fe(III) oxyhydroxides and the extent of microbial Fe(III) reduction in aquifer sediments. Here, the hydroxylamine-reducible Fe(III) in all samples was measured to indicate the potential microbially reducible Fe(III) of Al-Fe oxides. The results in Figure 7 show that hydroxylamine-reducible Fe(III) increased gradually with the Al content for samples synthesized at 300°C, 420°C, and 550°C, and the hydroxylamine-reducible Fe(III) of Al-Fe oxides synthesized at 180°C only increased from 0% to 20% Al content and then decreased with increasing Al content. The hydroxylamine-reducible Fe(III) also decreased as the synthesis temperature increased gradually from 180°C to 550°C for all the samples with different Al contents, except for the samples with higher Al content than 20% that had been sintered at 180°C. According to the XRD results in Figures 3 and 4, maghemite and hematite were the major crystalline phases for the Al-Fe samples. For the Al-Fe oxides with high sintering temperatures of 300°C, 420°C, and 550°C, a higher Al content would lead to lower crystallinity and higher BET surface areas of Fe oxides, resulting in the higher hydroxylamine-reducible Fe(III). It was reported that Al substitution has no effect on Fe(III) reduction in goethite and lepidocrocite, but increasing concentrations of Al in ferrihydrite result in decreasing microbial Fe(III) reduction (Ekstrom et al., 2010). For the samples with a sintering temperature of 180°C, no crystalline phase but likely an amorphous structure was observed as shown in Figure 3A when the Al contents were

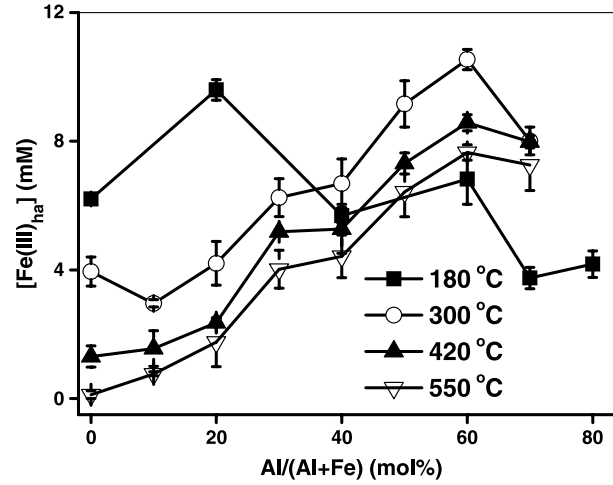

FIG. 7. Hydroxylamine-extractable Fe(III) concentrations of Al-Fe oxides synthesized at different temperatures versus Al/(Al + Fe) molar percentages: (A) 180°C, (B) 300°C, (C) 420°C, and (D) 550°C. Error bars represent the S.D. from the mean (n = 3).

high (≥60%). The increasing Al content in the Al-Fe oxides with such a low sintering temperature (180°C) also leads to the decreased hydroxylamine-reducible Fe(III).

Environmental Relevance and Implications

Iron redox cycling has a profound effect on the geochemistry of other elements (Hochella et al., 2008; Bose et al., 2009; Liu et al., 2014) and on the fates of contaminant metals (Lovley et al., 2004; Borch et al., 2010; Li et al, 2012b) and organic compounds (Li et al., 2009a, 2009b; Cao et al., 2010) in soil and sediments. However, Fe(III) (hydr)oxides are rarely pure in nature, and Al is one of most abundant metal elements on earth; Fe(III) (hydr)oxides are often coprecipitated with Al (Benny, 1998; Zhang et al., 2001; Cornell and Schwertmann, 2003). Faster Fe(III) reduction rates for ferrihydrite compared with more crystalline Fe(III) (hydr)oxides (Roden and Zachara, 1996; Glasauer et al., 2003) suggest that ferrihydrite is the most bioavailable, and thus important, Fe(III) phase for microbial respiration (Lovley and Phillips, 1986). Although increasing concentrations of Al in ferrihydrite have been found with decreasing microbial Fe(III) reduction, Al substitution has no effect on Fe(III) reduction in goethite and lepidocrocite minerals (Ekstrom et al., 2010). In our study, the results of hydroxylamine-reducible Fe(III) of Al-Fe oxides (180°C) also confirm the effects in which increasing Al content inhibits the Fe(III) reduction of low-crystallinity Fe oxides. In addition, the effects of the Al content on the Fe oxides with a higher degree of crystallization were also studied, but the results showed that the increasing Al content in these Fe oxides resulted in a significant enhancement of hydroxylamine-reducible Fe(III). As the Fe oxides with a high degree of crystallinity are also widespread in soils or sediments (Cornell and Schwertmann, 2003), these results suggest that the presence of Al will activate the Fe(III) in the structure and enhance the bioaccessibility of Fe(III), with a potential influence on the other elemental cycles or contaminant transformation.

Within mature soils and sediments, the preservation of low-crystallinity Fe oxyhydroxides (e.g., ferrihydrite, lepidocrocite, and goethite) will be a function of Al (or another cation) substitution (Wang et al., 1999; Hansel et al., 2011; Cristina et al., 2012; Bazilevskaya et al., 2012). The Al substitution can decrease iron bioaccessibility of Al-Fe oxides and produce more crystalline phases as preferential electron acceptors (Ekstrom et al., 2010). This study also showed that Al substitution can decrease the Fe (III) bioaccessibility of the maghemite synthesized at a low temperature (180°C), and the Al substitution significantly enhanced the Fe(III) bioaccessibility of Fe oxides synthesized at a high temperature (>300°C). This result confirms the conclusion that the Al-substituted highly crystallized Fe oxides in natural soils and sediments can be the primary terminal electron acceptors used by Fe(III)-reducing microorganisms, which play important roles in the *in situ* bioremediation of contaminated subsurface soils and sediments (Kukkadapu et al., 2006; Komlos et al., 2008). Thus, further exploration of the role of Al substitution in microbial Fe(III) reduction will be very helpful in predicting Fe bioaccessibility in soils or sediments and in the design of a potential Fe-based remediation approach for contaminated sites.

Although the nice correlations between the properties and the bioaccessibility of the laboratory-prepared Fe oxides are observed in this study, it has to be noted that the observations on the synthetic oxides may be different from the naturally occurring Fe oxides because of the complexity of the natural soils. To further extrapolate the current laboratory observations to the natural soil systems, it would be more representative to examine the characteristics and bioaccessibility of the synthesized complex Fe oxides and even the real soil samples.

CONCLUSIONS

Significant color changes were observed after increasing Al incorporation into Fe oxides, which was attributed to the absorbance changes of Al oxides and Fe oxides. The presence of alumina could hinder the crystallization of Fe oxides and crystal transformation from maghemite to hematite during sintering, and gibbsite with a high Al content was formed. The BET and micropore surface area increased significantly with increased alumina contents, but it decreased with an increased sintering temperature. The hydroxylamine-reducible Fe(III) of Al-substituted Fe oxides increased with increasing Al content for the Fe oxides with a high degree of crystallization but decreased with increasing Al content for Fe oxides with low crystallinity. Systematic characterizations of the crystal properties of Al-substituted Fe oxides and an evaluation of their bioaccessibility can provide fundamental information for understanding the biogeochemical role of Fe-Al–bearing minerals in artificial and natural soils or sediments.

REFERENCES

Bazilevskaya E., D. D. Archibald, and C. E. Martinez 2012. Rate constants and mechanisms for the crystallization of Al nano-goethite under environmentally relevant conditions. Geochim. Cosmochim. Acta 88:167–182.

Bazilevskaya E., D. D. Archibald, M. Aryanpour, J. D. Kubicki, and C. E. Martı′nez 2011. Aluminum coprecipitates with Fe (hydr)oxides: Does isomorphous substitution of Al^{3+} for Fe^{3+} in goethite occur? Geochim. Cosmochim. Acta 75:4667–4683.

Benny K. G. T. 1998. Chemistry of variable-charge soils. Soil Sci. 163:674–675.

Bonneville S., P. V. Cappellen, and T. Behrends 2004. Microbial reduction of iron (III) oxyhydroxides: Effects of mineral solubility and availability. Chem. Geol. 212:255–268.

Borch T., R. Kretzschmar, A. Kappler, P. V. Cappellen, M. Ginder-Vogel, A. Voegelin, and K. Campbell 2010. Biogeochemical redox processes and their impact on contaminant dynamics. Environ. Sci. Technol. 44:15–23.

Bose S., M. F. Hochella, Y. A. Gorby, D. W. Kennedy, D. E. McCready, A. S. Madden, and B. H. Lower 2009. Bioreduction of hematite nanoparticles by the dissimilatory iron reducing bacterium *Shewanella oneidensis* MR-1. Geochim. Cosmochim. Acta 73:962–976.

Bousserrhine N., U. G. Gasser, E. Jeanroy, and J. Berthelin 1999. Bacterial and chemical reductive dissolution of Mn-, Co-, Cr-, and Al-substituted goethites. Geomicrobiol. J. 16:245–258.

Cao F., F. B. Li, T. X. Liu, D. Y. Huang, C. Y. Wu, C. H. Feng, and X. M. Li 2010. Effect of *Aeromonas hydrophila* on reductive dechlorination of DDTs by zero-valent iron. J. Agric. Food. Chem. 58:12366–12372.

Cao F., T. X. Liu, C. Y. Wu, F. B. Li, X. M. Li, H. Y. Yu, H. Tong, and M. J. Chen 2012. Enhanced biotransformation of DDTs by an iron- and humic-reducing bacteria *Aeromonas hydrophila* HS01 upon addition of goethite and anthraquinone-2,6-disulphonic disodium salt (AQDS). J. Agric. Food Chem. 60:11238–11244.

Cornell R. M., and U. Schwertmann 2003. The Iron Oxides: Structure, Properties, Reactions, Occurrence and Uses. Weinheim, Germany, VCH.

Cristina C. A., M. F. Marc, J. F. Stebbins, L. Clement, and B. E. Gordon 2012. Properties of impurity-bearing ferrihydrite: I. Effects of Al content and precipitation rate on the structure of 2-line ferrihydrite. Geochim. Cosmochim. Acta 92:275–291.

Crosa M., V. Boero, and M. Franchini-Angela 1999. Determination of mean crystallite dimensions from X-ray diffraction peak profiles: A comparative analysis of synthetic hematites. Clays Clay Miner. 47:742–747.

Dominik P., H. N. Pohl, N. Bousserrhine, J. Berthelin, and M. Kaupenjohann 2002. Limitations to the reductive dissolution of Al-substituted goethites by *Clostridium butyricum*. Soil Biol. Biochem. 34:1147–1155.

Ekstrom E. B., D. R. Learman, A. S. Madden, and C. M. Hansel 2010. Contrasting effects of Al substitution on microbial reduction of Fe(III) (hydr)oxides. Geochim. Cosmochim. Acta 74:7086–7099.

Feng W., and C. J. Yapp 2009. Experimental tests of the effects of Al substitution on the goethite–water D H fractionation factor. Geochim. Cosmochim. Acta 72:1295–1311.

Fysh S. A., and P. M. Fredericks 1983. Fourier transform infrared studies of aluminous goethites and hematites. Clays Clay Miner. 31:377–382.

Gerke J. 2010. Humic (organic matter)-Al(Fe)-phosphate complexes: An underestimated phosphate form in soils and source of plant-available phosphate. Soil Sci. 175:417–425.

Glasauer S., P. G. Weidler, S. Langley, and T. J. Beveridge 2003. Controls on Fe reduction and mineral formation by a subsurface bacterium. Geochim. Cosmochim. Acta 67:1277–1288.

Hansel C. M., D. R. Learman, C. J. Lentini, and E. B. Ekstrom 2011. Effect of adsorbed and substituted Al on Fe(II)-induced mineralization pathways of ferrihydrite. Geochim. Cosmochim. Acta 75:4653–4666.

Hochella M. F., S. K. Lower, P. A. Maurice, R. L. Penn, N. Sahai, D. L. Sparks, and B. S. Twining 2008. Nanominerals, mineral nanoparticles, and Earth systems. Science 319:1631–1635.

Kappler A., and K. L. Straub 2005. Geomicrobiological cycling of iron. Rev. Mineral. Geochem. 59:85–108.

Komlos J., A. Peacock, R. K. Kukkadapu, and P. R. Jaffe 2008. Long-term dynamics of uranium reduction/reoxidation under low sulfate conditions. Geochim. Cosmochim. Acta 72:3603–3615.

Kukkadapu R. K., J. M. Zachara, J. K. Fredrickson, J. P. McKinley, D. W. Kennedy, S. C. Smith, and H. Dong 2006. Reduction biotransformation of Fe in shale-limestone saprolite containing Fe(III) oxides and Fe(II)/Fe(III) phyllosilicates. Geochim. Cosmochim. Acta 70:3662–3676.

Kukkadapu R. K., J. M. Zachara, S. C. Smith, J. K. Fredrickson, and C. Liu 2001. Dissimilatory bacterial reduction of Al-substituted goethite in subsurface sediments. Geochim. Cosmochim. Acta 65:2913–2924.

Lair G. J., F. Zehetner, M. Hrachowitz, N. Franz, F.-J. Maringer, and M. H. Gerzabek 2009. Dating of soil layers in a young floodplain using iron oxide crystallinity. Quat. Geochronol. 4:260–266.

Li F. B., X. M. Li, S. G. Zhou, L. Zhuang, F. Cao, D. Y. Huang, W. Xu, T. X. Liu, and C. H. Feng 2010. Enhanced reductive dechlorination of DDT in an anaerobic system of dissimilatory iron-reducing bacteria and iron oxide. Environ. Pollut. 158:1733–1740.

Li J. Y., and R. K. Xu 2013. Inhibition of acidification of kaolinite and an alfisol subsoil by iron oxides through electrical double-layer interaction. Soil Sci. 178:37–45.

Li J., and D. D. Richter 2012. Effects of two-century land use changes on soil iron crystallinity and accumulation in Southeastern Piedmont region, USA. Geoderma 173–174:184–191.

Li X. M., L. Liu, T. X. Liu, T. Yuan, W. Zhang, F. B. Li, S. G. Zhou, and Y. T. Li 2013. Electron transfer capacity dependence of quinone-mediated Fe(III) reduction and current generation by *Klebsiella pneumoniae* L17. Chemosphere 92:218–224.

Li X. M., S. G. Zhou, F. B. Li, C. Y. Wu, L. Zhuang, W. Xu, and L. Liu 2009a. Fe(III) oxide reduction and carbon tetrachloride dechlorination by a newly isolated *Klebsiella pneumoniae* strain L17. J. Appl. Microbiol. 106:130–139.

Li X. M., T. X. Liu, F. B. Li, W. Zhang, S. G. Zhou, and Y. T. Li 2012a. Reduction of structural Fe(III) in oxyhydroxides by *Shewanella decolorationis* S12 and characterization of the surface properties of iron minerals. J. Soil Sediment 379:143–150.

Li X. M., T. X. Liu, L. Liu, and F. B. Li 2014. Dependence of the electron transfer capacity on the kinetics of quinone-mediated Fe(III) reduction by two iron/humic reducing bacteria. RSC Adv. 4:2284–2290.

Li X. M., T. X. Liu, N. M. Zhang, G. Ren, F. B. Li, and Y. T. Li 2012b. Effect of Cr(VI) on Fe(III) reduction in three paddy soils from the Hani terrace field at high altitude. Appl. Clay Sci. 64:53–60.

Li X. M., Y. T. Li, F. B. Li, S. G. Zhou, C. H. Feng, and T. X. Liu 2009b. Interactively interfacial reaction of iron-reducing bacterium and goethite for reductive dechlorination of chlorinated organic compounds. Chin. Sci. Bull. 54:2800–2804.

Liu H., T. Chen, X. Zou, C. Qing, and R. L. Frost 2013. Thermal treatment of natural goethite: Thermal transformation and physical properties. Thermochim. Acta 568:115–121.

Liu T. X., X. M. Li, F. B. Li, W. Zhang, M. J. Chen, and S. G. Zhou 2011. Reduction of iron oxides by *Klebsiella pneumoniae* L17: Kinetics and surface properties. Colloids Surf. A Physicochem. Eng. Aspects 379:143–150.

Liu T. X., X. M. Li, W. Zhang, M. Hu, and F. B. Li 2014. Fe(III) oxides accelerating microbial nitrate reduction and electricity generation by *Klebsiella pneumoniae* L17. J. Colloid Interf. Sci. 423:25–32.

Lovley D. R., and E. J. P. Phillips 1987. Rapid assay for microbially reducible ferric iron in aquatic sediments. Appl. Environ. Microbiol. 53:1536–1540.

Lovley D. R., D. E. Holmes, and K. P. Nevin 2004. Dissimilatory Fe(III) and Mn (IV) reduction. Adv. Microb. Physiol. 49:219–286.

Lovley D. R., and E. J. P. Phillips 1986. Organic matter mineralization with reduction of ferric iron in anaerobic sediments. Appl. Environ. Microbiol. 51:683–689.

Masue Y., R. H. Loeppert, and T. A. Kramer 2007. Arsenate and arsenite adsorption and desorption behavior on coprecipitated aluminum:iron hydroxides. Environ. Sci. Technol. 41:837–842.

Maurice P. A., Y. J. Lee, and L. E. Hersman 2000. Dissolution of Al-substituted goethites by an aerobic *Pseudomonas mendocina* var. bacteria. Geochim. Cosmochim. Acta 64:1363–1374.

Melnikov P., V. A. Nascimento, I. V. Arkhangelsky, L. Z. Zanoni Consolo, and L. C. S. de Oliveira 2014. Thermal decomposition mechanism of iron(III) nitrate and characterization of intermediate products by the technique of computerized modeling. J. Therm. Anal. Calorim. 115:145–151.

Roden E. E., and J. M. Zachara 1996. Microbial reduction of crystalline iron(III) oxides: Influence of oxide surface area and potential for cell growth. Environ. Sci. Technol. 30:1618–1628.

Schwertmann U., and R. M. Cornell 1991. Iron oxides in the laboratory: Preparation and characterization. New York, NY, VCH.

Torrent J., and V. Barron 2003. The visible diffuse reflectance spectrum in relation to the color and crystal properties of hematite. Clays Clay Miner. 51:309–317.

Trolard F., and Y. Tardy 1987. The stabilities of gibbsite, boehmite, aluminous goethites and aluminous hematites in bauxites, ferricretes, and laterites as a function of water activity, temperature, and particle size. Geochim. Cosmochim. Acta 51:945–957.

Verdú-Andrés J., F. Bosch-Reig, and P. Campíns-Falcó 1998. Analyte estimation using the generalized H-point standard additions method and a new methodology for locating linear spectral intervals for unknown interferents. J. Chemometrics 12:27–40.

Wahbi A. A., E. Hassan, M. Barary, E. Khamis, and D. Hamdi 2007. Derivative spectrophotometry in the visible region using absorbance versus log wavelength or wavenumber determination of cyanocobalamin in injection solutions. Pak. J. Pharm. Sci. 20:93–99.

Wang M. K., C. M. Chang, Y. W. Cheng, and K. H. Houng 1999. Comparison of synthetic and soil Al-substituted lepidocrocite. Soil Sci. 164:311–321.

Wu Y. D., T. X. Liu, X. M. Li, and F. B. Li 2014. Exogenous electron shuttle-mediated extracellular electron transfer of *Shewanella putrefaciens* 200: Electrochemical parameters and thermodynamics. Environ. Sci. Technol. 48:9306–9314.

Zhang M., A. K. Alva, Y. C. Li, and D. V. Calvert 2001. Aluminum and iron fractions affecting phosphorus solubility and reactions in selected sandy soils. Soil Sci. 166:940–948.

Zhang W., X. M. Li, T. X. Liu, and F. B. Li 2012. Enhanced nitrate reduction and current generation by *Bacillus sp*. in the presence of iron oxides. J. Soil. Sediment. 12:354–365.

Zhang W., X. M. Li, T. X. Liu, F. B. Li, and W. J. Shen 2014. Competitive reduction of nitrate and iron oxides by *Shewanella putrefaciens* 200 under anoxic conditions. Colloids Surf. A Physicochem. Eng. Aspects 445:97–104.

Zhu B., B. Fang, and X. Li 2010. Dehydration reactions and kinetic parameters of gibbsite. Ceram. Int. 36:2493–2498.